

# What the Milky Way bulge reveals about the initial metallicity gradients in the disc

F. Fragkoudi<sup>1</sup>, P. Di Matteo<sup>1</sup>, M. Haywood<sup>1</sup>, S. Khoperskov<sup>1</sup>, A. Gómez<sup>1</sup>, M. Schultheis<sup>2</sup>, F. Combes<sup>3,4</sup>, and B. Semelin<sup>3</sup>

<sup>1</sup> GEPI, Observatoire de Paris, PSL Research University, CNRS, Place Jules Janssen, 92195, Meudon, France  
e-mail: francesca.fragkoudi@obspm.fr

<sup>2</sup> Laboratoire Lagrange, Université Côte d'Azur, Observatoire de la Côte d'Azur, CNRS, Bd de l'Observatoire, 06304 Nice, France

<sup>3</sup> Observatoire de Paris, LERMA, CNRS, PSL Univ., UPMC, Sorbonne Univ., F-75014, Paris, France

<sup>4</sup> College de France, 11 Place Marcelin Berthelot, 75005, Paris, France

## ABSTRACT

We examine the metallicity trends in the Milky Way (MW) bulge – using APOGEE DR13 data – and explore their origin by comparing two N-body models of isolated galaxies which develop a bar and a boxy/peanut (b/p) bulge. Both models have been proposed as scenarios for reconciling a disc origin of the MW bulge with a negative vertical metallicity gradient. The first model is a superposition of co-spatial, i.e. overlapping, disc populations with different scaleheights, kinematics and metallicities. In this model the thick, metal-poor, and centrally concentrated disc populations contribute significantly to the stellar mass budget in the inner galaxy. The second model is a single disc with an initial steep radial metallicity gradient, which is mapped by the bar into the b/p bulge in such a way that the vertical metallicity gradient of the MW bulge is reproduced – as shown already in previous works in the literature. However, as we show here, the latter model does not reproduce the positive longitudinal metallicity gradient of the inner disc, nor the metal-poor innermost regions of the Bulge seen in the data. On the other hand, the model with co-spatial thin and thick disc populations reproduces all the aforementioned trends. We therefore see that it is possible to reconcile a (primarily) disc origin for the MW bulge with the observed trends in metallicity by mapping the inner thin and thick discs of the MW into a b/p. For this scenario to reproduce the observations, the  $\alpha$ -enhanced, metal-poor, thick disc populations must have a significant mass contribution in the inner regions – as has been suggested for the Milky Way.

**Key words.** Galaxy: bulge - Galaxy: disc - Galaxy: structure

## 1. Introduction

By examining the Milky Way (MW) bulge, its morphology, chemistry and kinematics, we can hope to disentangle its formation history (e.g. Calura et al. 2012; Obreja et al. 2013) and the origin of its various stellar populations (as revealed by its broad metallicity distribution function, MDF; McWilliam & Rich 1994; Hill et al. 2011; Ness et al. 2013; Rojas-Arriagada et al. 2014; Zoccali et al. 2017).

In terms of morphology, it is well established that the Bulge has a characteristic X-shape, as can be seen from images in the near- and mid-infrared (Dwek et al. 1995; Ness & Lang 2016) and evidenced by the split in the red clump magnitude distribution (McWilliam & Zoccali 2010). This is interpreted as being due to the presence of a boxy/peanut (b/p) bulge, a structure which forms due to the vertical heating of stellar bars through resonances and/or the buckling instability (Combes & Sanders 1981; Combes et al. 1990; Raha et al. 1991; Athanassoula 2005; Martinez-Valpuesta et al. 2006; Quillen et al. 2014). The Bulge is therefore thought to have, at least partly, a disc origin, and will be made up of material from within the inner disc out to the Outer Lindblad Resonance (OLR; values for the present day OLR range between  $\sim 8$ -10 kpc - see e.g. Bland-Hawthorn & Gerhard 2016), which are the stars that are thought to participate in building up the bar and the b/p bulge (Di Matteo et al. 2014; Halle et al. 2015).

Regarding the chemistry of the MW bulge, it is now well known that it has a negative vertical metallicity gradient (Minniti et al. 1995; Zoccali et al. 2008; Johnson et al. 2011; Gonzalez et al. 2013) due to the changing contribution of different stellar populations above the plane, i.e., the fraction of metal-poor stars ( $[Fe/H] \leq 0$ ) increases as we move further away from the plane of the Galaxy, while the fraction of metal-rich stars ( $[Fe/H] \geq 0$ ) decreases (e.g. Ness et al. 2013; Rojas-Arriagada et al. 2014). This vertical metallicity gradient was originally thought to be incompatible with a pure disc scenario for the MW bulge, and a dispersion-dominated classical bulge/spheroid was invoked to explain it (e.g. Zoccali et al. 2008). However, subsequent work showed that the kinematics of the MW bulge are incompatible with the presence of a *massive* classical bulge - as it would need to be in order to explain the vertical metallicity gradient (e.g. Shen et al. 2010; Kunder et al. 2012; Di Matteo et al. 2014; Debattista et al. 2017; upper limit between 2-10% of the total stellar mass). While Saha et al. (2012) showed that classical bulges can be spun-up by bars, it is not evident that *massive* classical bulges could acquire the rotation required to “hide” them kinematically (see e.g. Fux 1997; Di Matteo et al. 2014).

Martinez-Valpuesta & Gerhard (2013), showed that it is possible to reconcile the vertical gradient with a disc-origin of the bulge when the pre-existing disc has a steep initial radial metallicity gradient (see also Bekki & Tsujimoto 2011). They showed

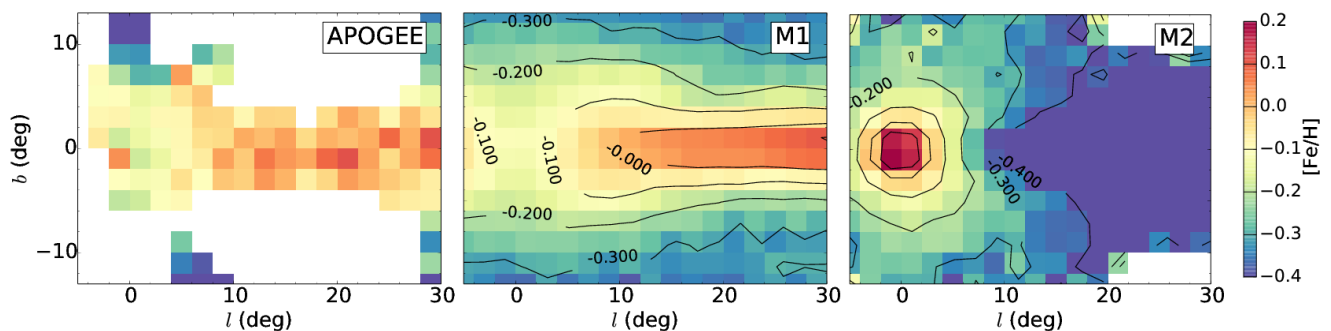


**Fig. 1.** Mean metallicity along the line of sight as a function of galactic longitude  $l$  and galactic latitude  $b$  for the APOGEE DR13 data (left), model M1 (middle) and model M2 (right). For the observed (theoretical) map only stars (particles) with distances between 4 and 12 kpc from the Sun are selected. Only pixels with more than 10 stars (particles) are shown. Each bin is 2 degrees in  $l$  and  $b$ . The black contour lines correspond to iso-metallicity contours, as labeled on the colourbar.

that this steep radial gradient is mapped<sup>1</sup> by the bar into the  $b/p$  in such a way that the bulge recovers a vertical metallicity gradient. This is due to the fact that while stars from most of the disc participate in the formation of the  $b/p$ , stars from larger galactocentric radii will preferentially get mapped into the bulge at larger heights above the plane (Martinez-Valpuesta & Gerhard 2013; Di Matteo et al. 2014). Di Matteo et al. (2015) later-on showed that while the above scenario can reproduce the global kinematic properties of the MW bulge, this model does not reproduce the kinematics of separate stellar populations, i.e. when the stars are separated according to their metallicity (see Di Matteo et al. 2015 for more details).

Another scenario which has been proposed for reconciling the disc origin of the MW bulge with its vertical metallicity gradient – while also reproducing morphological and kinematic properties of the MW bulge – is one in which the metal-poor,  $\alpha$ -enhanced stars in the bulge are part of the same population as the thick disc stars at the solar vicinity (Bekki & Tsujimoto 2011; Di Matteo et al. 2015; Di Matteo 2016; Athanassoula et al. 2017; Fragkoudi et al. 2017). In this scenario the  $\alpha$ -enhanced thick disc would have to be overall quite massive (as asserted by Snaith et al. 2015; Haywood et al. 2015) and centrally concentrated, i.e. with a short scalelength (as shown by Bensby et al. 2011; Bovy et al. 2012 and see table A) therefore being a dominant component of the inner MW. In this framework, the bulge is not an exclusively old population, but rather has a spread in ages – as has indeed been suggested by recent studies (e.g. Bensby et al. 2013, 2017; Haywood et al. 2016a). In this context, the vertical metallicity gradient is present in the disc even before the  $b/p$  bulge forms and is enhanced by the way the bar maps the thin and thick disc populations into the  $b/p$  bulge.

In this letter we explore the metallicity trends arising in the two aforementioned “pure disc” models, and compare them with data from the infrared APOGEE survey (Majewski et al. 2015), which can probe stellar populations close to the plane of the inner MW. We show that while the model with an initial steep radial gradient can reproduce the vertical gradient of the MW bulge, it cannot reproduce the longitudinal gradient in the inner MW nor the average metallicity in the innermost regions. This hints at the lack of an initial steep radial metallicity gradient in the MW disc at the time the bar buckled to form the  $b/p$  bulge. On the other hand, we show that the model with co-spatial thin and thick discs, which are mapped into the bulge by the bar, can

naturally reproduce all the aforementioned trends; in particular, the low mean metallicity ( $[Fe/H] \sim -0.1$ ) observed in the inner few degrees of the MW bulge can be reproduced in a pure disc scenario, with no real need for any additional massive component – such as a classical bulge.

## 2. Simulations

### 2.1. M1: Co-spatial discs

In this model<sup>2</sup> we discretise the vertically continuous stellar populations seen in the MW inner disc (see Bovy et al. 2012, Figure 5) into three co-spatial i.e. overlapping, discs:  $D1$ ) a thin, kinematically cold, metal-rich disc ( $[Fe/H] > 0$ ), associated with the metal-rich thin disc seen in the solar vicinity,  $D2$ ) an intermediate disc with intermediate kinematics and metallicities ( $0 > [Fe/H] > -0.5$ ), which is associated to the young thick disc, and  $D3$ ) a kinematically hot and metal-poor disc ( $-0.5 > [Fe/H] > -1$ ) with scaleheight and kinematic properties corresponding to the old thick disc seen at the Solar vicinity (nomenclature as in Haywood et al. 2013).

Disc particles are assigned a metallicity by drawing randomly from a normal distribution, where each disc has a mean metallicity and dispersion (see table A), assigned such that we can reproduce the MDF of the inner MW (Haywood et al., submitted). Discs  $D2$  and  $D3$  are assigned a flat radial metallicity gradient, since we assume that the ISM was well-mixed at the time the young and old thick disc formed ( $z > 1$ ), due to a high star formation rate ( $> 10 M_{\odot}/\text{yr}$ ), meaning that the galaxy was likely in a bursty and turbulent state (Lehnert et al. 2014; Wuyts et al. 2016; Ma et al. 2017, but see also Pilkington et al. 2012). The thin disc ( $D1$ ) is associated to the final more quiescent phase of the MW in the last  $\sim 7$ -8 Gyr (see Snaith et al. 2014; Haywood et al. 2016b). We are only interested in the gradient of the *inner* thin disc, since the outer disc does not participate in the  $b/p$  bulge. While it is possible that the inner thin disc could have a negative gradient, we investigate the simplest case first, i.e. a flat gradient. The combined mass of  $D2$  and  $D3$  (young and old thick) discs is  $\sim 50\%$  of the total stellar mass in the model, and the other  $\sim 50\%$  is in the thin disc component, in agreement with the mass growth of the MW disc as estimated by Snaith et al. (2014, 2015).

The fact that  $D2$  and  $D3$  have a larger scaleheight than the thin disc leads to a global negative vertical metallicity gradient

<sup>1</sup> Note that here and in what follows, when we say that the bar “maps” stars into the  $b/p$ , we mean that disc stars are redistributed by the bar into the  $b/p$  bulge.

<sup>2</sup> The main properties of the two models are summarised here. For a more detailed description see Appendix A.

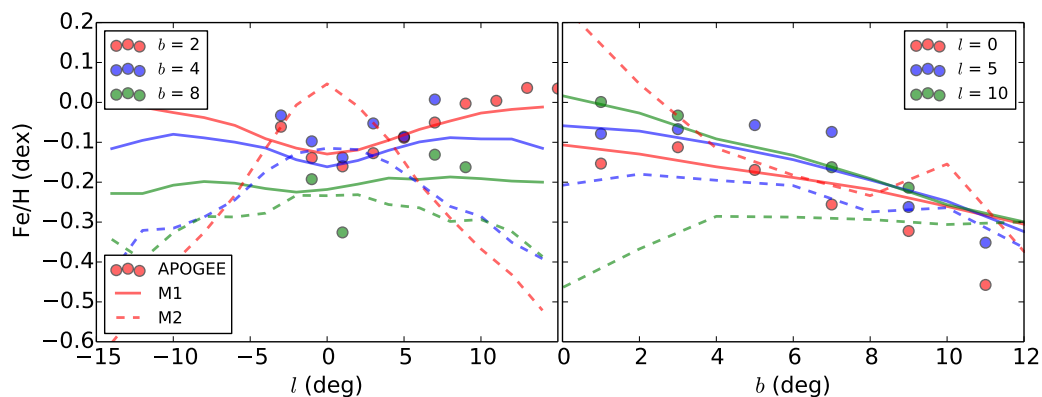


**Fig. 2.** *Left:* Mean metallicity as a function of longitude for different cuts in latitude as indicated in the legend. *Right:* Mean metallicity as a function of latitude for different cuts in longitude as indicated in the legend. The solid line corresponds to Model M1 while the dashed line corresponds to Model M2. The circles correspond to data from APOGEE. For the observations (models) only stars (particles) with distances between 4 and 12 kpc from the Sun are considered.

at the start of the simulation (see left column Figure B.1). The model represents the inner MW (i.e. up to the OLR  $\sim 8$ -10 kpc - see e.g. Bland-Hawthorn & Gerhard 2016). The model is evolved over secular timescales, i.e. 7 Gyr until a bar and b/p form, and in what follows, we analyse a snapshot from the end of the simulation which is re-scaled so that the bar has a length of  $\sim 4.5$  kpc (similar to the length of the MW bar, e.g. Bland-Hawthorn & Gerhard 2016).

## 2.2. M2: Radial metallicity gradient

In this model (M2) we employ a single stellar disc which has an initial steep radial metallicity gradient. The particles are assigned a metallicity as a function of their initial radius in the disc according to  $[\text{Fe}/\text{H}] = [\text{Fe}/\text{H}]_0 + \text{grad} \times r$ , where  $\text{grad} = -0.4 \text{ dex/kpc}$  and  $[\text{Fe}/\text{H}]_0 = 0.6 \text{ dex}$ , in order to emulate the models explored in Martinez-Valpuesta & Gerhard (2013) and Di Matteo et al. (2015). The model is evolved over secular timescales for 9 Gyr and in what follows we analyse the final snapshot which is re-scaled so that the bar has a length of  $\sim 4.5$  kpc - similar to the MW bar length.

## 3. Results

In Figure 1 we explore the mean metallicity  $[\text{Fe}/\text{H}]$  along the line of sight in galactic longitude  $l$ , and galactic latitude  $b$ , for the two models described above, taking particles which are in the bar/bulge region with distances between 4 and 12 kpc from the Sun (the Sun is placed at 8 kpc from the centre and the bar has an angle of 30 degrees to the galactocentric line of sight). We compare these to a mean metallicity map of the inner MW constructed with data from APOGEE DR13 (Majewski et al. 2015; SDSS Collaboration et al. 2016), where stars are selected to have distances between 4 and 12 kpc from the Sun. The distances are taken from Wang et al. (2016) (see also their section 3 for more details on how stars in this sample are selected), and we apply an additional cut on surface gravity,  $\log g > 0.5$ , to remove biases from the most distant metal-poor stars in the bulge (see section 5.1 in Ness et al. 2016). Only bins with more than 10 stars are shown (bins are  $2 \times 2$  deg), and the total number of stars used to construct this map is  $\sim 7300$ .

We see that model M1 (middle panel Figure 1), is able to reproduce the vertical metallicity gradient, seen also in the

APOGEE data (left panel Figure 1), due to the changing contribution of the different populations with latitude (see the right column of Figure B.2 where we show the fractional contribution of the three co-spatial populations in  $l, b$  for this snapshot.) Model M2 (right panel Figure 1), also reproduces the vertical metallicity gradient due to the fact that stars which are further out in the disc are mapped at larger distances above the plane by the bar in the b/p bulge (see Martinez-Valpuesta & Gerhard 2013 and Di Matteo et al. 2014). However, the two models give very different predictions for the longitudinal metallicity gradient. We see that M1's inner disc ( $30 > l > 10$ ) is metal-rich close to the plane, due to the fact that the thin metal-rich disc is concentrated in the plane of the galaxy, as can be seen in the right column of Figure B.2 (it contributes  $\sim 60\%$  of the surface density for  $b < |5|$ ). On the other hand, in Figure 1, we see that M2 predicts a metal-poor inner disc at longitudes  $l > 10$  degrees. These are diametrically opposite predictions, in the sense that M1 predicts a positive longitudinal gradient while M2 predicts a negative longitudinal gradient, and we see from the APOGEE data that M1 can reproduce the data much better than M2.

Furthermore, the models also give different predictions for the mean metallicity in the inner regions; M1 predicts relatively low metallicity inside  $|l, b| < 5$  deg, of the order of  $-0.1$  dex, while M2 predicts that metallicity will be highest in the centre, on the order of  $0.1$  dex. We see that M1 is compatible with the APOGEE data which points to low metallicities, on average  $\sim -0.1$  dex (and see also Zoccali et al. 2017).

The relation between the models and the data can be further explored by examining Figure 2. In the left panel we show metallicity as a function of longitude for different cuts in  $b$  as indicated in the inset. We see that M1 (solid lines) predicts increasing metallicity towards larger longitudes with a dip in the centre (at  $l=0$ ), whereas M2 (dashed lines) predicts decreasing metallicity with a peak in the centre. For the APOGEE data (circles) the error on the mean for the data is smaller than the points and therefore is not shown. We see that there is a very good agreement between the *trends* for model M1 and the data, especially close to the plane. i.e. for  $b=2$ , while model M2 is essentially excluded. It is interesting to note that the data seem to show an inversion of metallicities compared to the models, around  $l=0$ , for  $b=2$  and 4 (i.e.  $b=2$  seems to be more metal-poor than  $b=4$ , contrary to the prediction of both the models). Since both models are pure discs, this could possibly hint at the existence of a small, concentrated classical bulge, or a contribution from the stellar halo,

which make the very innermost region of the MW more metal-poor. In the right panel of Figure 2 we show the metallicity as a function of  $b$  for different cuts in longitude, where the negative vertical gradient is clearly seen in the data. We note that the metallicity in the model does not decrease as rapidly as in the data, due to a larger fraction of metal-rich stars at high latitudes. This occurs because we do not have star formation in the model and thus all cold, metal-rich populations, are present before the bar buckling episode. Notwithstanding, the main trends in the data are well reproduced by the model.

#### 4. Discussion & Conclusions

We examine metallicity trends in the Milky Way bulge using APOGEE data, and explore their origin by revisiting a scenario which has been proposed as a way of reconciling the “pure disc” nature of the MW bulge with its negative vertical metallicity gradient (model M2), and comparing it to another recently proposed scenario (model M1). Model M1 has co-spatial stellar populations which are represented by a thin, kinematically cold metal-rich disc ( $[\text{Fe}/\text{H}] > 0$ ), an intermediate disc in terms of thickness, kinematics and metallicity ( $-0.5 < [\text{Fe}/\text{H}] < 0$ ) and a thicker, kinematically hotter metal-poor disc ( $-1 < [\text{Fe}/\text{H}] < -0.5$ ), where the intermediate and thick discs, i.e. the metal-poor populations, make up approximately 50% of the stellar mass and are centrally concentrated. Model M2 has a single disc with an initial steep radial metallicity gradient ( $-0.4 \text{ dex/kpc}$ ) and no initial vertical gradient. Both models are evolved in isolation and develop a bar which buckles to form a boxy/peanut bulge.

While the bar in model M2 maps the initial steep radial gradient into a negative vertical metallicity gradient in the b/p bulge – thus producing a negative vertical gradient (as already shown in Martínez-Valpuesta & Gerhard 2013 and Di Matteo et al. 2014) – it fails to reproduce the positive longitudinal metallicity gradient close to the plane, as well as the mean metallicity in the innermost regions of the MW bulge (inside  $|l, b| < 5 \text{ deg}$ ) – which can now be observed thanks to the infrared APOGEE survey. On the other hand, we see that M1 is able to reproduce all the aforementioned trends in the data.

The inability of model M2 to reproduce all the trends in the MW bulge hints at the lack of a steep radial metallicity gradient in the inner MW at the time the bar buckled to form the b/p bulge. This is in line with recent observational (e.g. Wuyts et al. 2016) and theoretical studies which show that a large fraction of galaxies at high redshifts have flat gas-phase metallicity gradients due to strong feedback and disc-disturbing processes such as rapid gas infall (e.g. Gibson et al. 2013; Ma et al. 2017). While we do not exclude that the inner MW could have had an initial shallow negative radial gradient, according to our results, it had to be flatter than the one of M2. On the other hand, if the initial radial gradient is less steep than in model M2, the vertical gradient produced in the b/p bulge will not be as steep as is required by the data. Therefore, there must be another scenario able to produce the fairly steep negative vertical gradient observed in the MW bulge, while also satisfying the rest of its chemical, morphological and kinematic trends.

As mentioned, model M1 is able to naturally reproduce both the vertical and longitudinal metallicity gradients seen in the APOGEE data, as well as the metal-poor inner region ( $|l, b| < 5 \text{ deg}$ ) of the MW bulge. Our findings suggest that the stellar populations that make up the inner MW arose from an ISM which was well mixed and turbulent, and whose radial metallicity gradients were mostly flat (Haywood et al. 2013; Nidever et al. 2014; Feng & Krumholz 2014; Di Matteo et al. 2015; Haywood et al. 2015;

Wuyts et al. 2016; Di Matteo 2016), with stars first forming in a geometrically thick layer, and then in thinner layers in an upside-down fashion (e.g. Bird et al. 2013). In such a model, where the MW bulge forms via the bar mapping the thin and thick inner disc populations into a b/p bulge, it is not necessary to add any other massive components to the model in order to reproduce the trends in metallicity (such as a classical bulge/spheroid), nor is an initial radial metallicity gradient in the disc needed.

*Acknowledgements.* This work has been supported by the ANR (Agence Nationale de la Recherche) through the MOD4Gaia project (ANR-15-CE31-0007, P.I.: P. Di Matteo). FF is supported by a postdoctoral grant from the Centre National d’Etudes Spatiales (CNES). This work was granted access to the HPC resources of CINES under the allocation 2016-040507 made by GENCI.

#### References

- Athanassoula, E. 2005, *MNRAS*, 358, 1477  
 Athanassoula, E., Rodionov, S. A., & Prantzos, N. 2017, *MNRAS*, 467, L46  
 Barnes, J. & Hut, P. 1986, *Nature*, 324, 446  
 Bekki, K. & Tsujimoto, T. 2011, *MNRAS*, 416, L60  
 Bensby, T., Alves-Brito, A., Oey, M. S., Yong, D., & Meléndez, J. 2011, *ApJ*, 735, L46  
 Bensby, T., Feltzing, S., Gould, A., et al. 2017, *A&A*, 605, A89  
 Bensby, T., Yee, J. C., Feltzing, S., et al. 2013, *A&A*, 549, A147  
 Binney, J. & Tremaine, S. 2008, *Galactic Dynamics*, 2nd edn. (Princeton University Press), 920  
 Bird, J. C., Kazantzidis, S., Weinberg, D. H., et al. 2013, *ApJ*, 773, 43  
 Bland-Hawthorn, J. & Gerhard, O. 2016, *ARA&A*, 54, 529  
 Boyy, J., Rix, H.-W., Liu, C., et al. 2012, *ApJ*, 753, 148  
 Calura, F., Gibson, B. K., Michel-Dansac, L., et al. 2012, *MNRAS*, 427, 1401  
 Combes, F., Debbasch, F., Friedli, D., & Pfenniger, D. 1990, *A&A*, 233, 82  
 Combes, F. & Sanders, R. H. 1981, *A&A*, 96, 164  
 Debattista, V. P., Ness, M., Gonzalez, O. A., et al. 2017, *MNRAS*, 469, 1587  
 Di Matteo, P. 2016, *PASA*, 33, e027  
 Di Matteo, P., Gómez, A., Haywood, M., et al. 2015, *A&A*, 577, A1  
 Di Matteo, P., Haywood, M., Gómez, A., et al. 2014, *A&A*, 567, A122  
 Dwek, E., Arendt, R. G., Hauser, M. G., et al. 1995, *ApJ*, 445, 716  
 Feng, Y. & Krumholz, M. R. 2014, *Nature*, 513, 523  
 Fragkoudi, F., Di Matteo, P., Haywood, M., et al. 2017, *ArXiv e-prints* [arXiv:1704.00734]  
 Fux, R. 1997, *A&A*, 327, 983  
 Gibson, B. K., Pilkington, K., Brook, C. B., Stinson, G. S., & Bailin, J. 2013, *A&A*, 554, A47  
 Gonzalez, O. A., Rejkuba, M., Zoccali, M., et al. 2013, *A&A*, 552, A110  
 Halle, A., Di Matteo, P., Haywood, M., & Combes, F. 2015, *A&A*, 578, A58  
 Haywood, M., Di Matteo, P., Lehnert, M. D., Katz, D., & Gómez, A. 2013, *A&A*, 560, A109  
 Haywood, M., Di Matteo, P., Snaith, O., & Calamida, A. 2016a, *A&A*, 593, A82  
 Haywood, M., Di Matteo, P., Snaith, O., & Lehnert, M. D. 2015, *A&A*, 579, A5  
 Haywood, M., Lehnert, M. D., Di Matteo, P., et al. 2016b, *A&A*, 589, A66  
 Hill, V., Lecœur, A., Gómez, A., et al. 2011, *A&A*, 534, A80  
 Johnson, C. I., Rich, R. M., Fulbright, J. P., Valenti, E., & McWilliam, A. 2011, *ApJ*, 732, 108  
 Kunder, A., Koch, A., Rich, R. M., et al. 2012, *AJ*, 143, 57  
 Lehnert, M. D., Di Matteo, P., Haywood, M., & Snaith, O. N. 2014, *ApJ*, 789, L30  
 Ma, X., Hopkins, P. F., Feldmann, R., et al. 2017, *MNRAS*, 466, 4780  
 Majewski, S. R., Schiavon, R. P., Frinchaboy, P. M., et al. 2015, *ArXiv e-prints* [arXiv:1509.05420]  
 Martínez-Valpuesta, I. & Gerhard, O. 2013, *ApJ*, 766, L3  
 Martínez-Valpuesta, I., Shlosman, I., & Heller, C. 2006, *ApJ*, 637, 214  
 McWilliam, A. & Rich, R. M. 1994, *ApJS*, 91, 749  
 McWilliam, A. & Zoccali, M. 2010, *ApJ*, 724, 1491  
 Minniti, D., Olszewski, E. W., Liebert, J., et al. 1995, *MNRAS*, 277, 1293  
 Ness, M., Freeman, K., Athanassoula, E., et al. 2013, *MNRAS*, 430, 836  
 Ness, M. & Lang, D. 2016, *AJ*, 152, 14  
 Ness, M., Zasowski, G., Johnson, J. A., et al. 2016, *ApJ*, 819, 2  
 Nidever, D. L., Boyy, J., Bird, J. C., et al. 2014, *ApJ*, 796, 38  
 Obreja, A., Domínguez-Tenreiro, R., Brook, C., et al. 2013, *ApJ*, 763, 26  
 Pilkington, K., Few, C. G., Gibson, B. K., et al. 2012, *A&A*, 540, A56  
 Quillen, A. C., Minchev, I., Sharma, S., Qin, Y.-J., & Di Matteo, P. 2014, *MNRAS*, 437, 1284  
 Raha, N., Sellwood, J. A., James, R. A., & Kahn, F. D. 1991, *Nature*, 352, 411  
 Rodionov, S. A., Athanassoula, E., & Sotnikova, N. Y. 2009, *MNRAS*, 392, 904  
 Rojas-Arriagada, A., Recio-Blanco, A., Hill, V., et al. 2014, *A&A*, 569, A103  
 Saha, K., Martínez-Valpuesta, I., & Gerhard, O. 2012, *MNRAS*, 421, 333  
 SDSS Collaboration, Albareti, F. D., Allende Prieto, C., et al. 2016, *ArXiv e-prints* [arXiv:1608.02013]  
 Semelin, B. & Combes, F. 2002, *A&A*, 388, 826  
 Shen, J., Rich, R. M., Kormendy, J., et al. 2010, *ApJ*, 720, L72  
 Snaith, O., Haywood, M., Di Matteo, P., et al. 2015, *A&A*, 578, A87  
 Snaith, O. N., Haywood, M., Di Matteo, P., et al. 2014, *ApJ*, 781, L31  
 Wang, J., Shi, J., Pan, K., et al. 2016, *MNRAS*, 460, 3179  
 Wuyts, E. et al. 2016, *ApJ*, 827, 74  
 Zoccali, M., Hill, V., Lecœur, A., et al. 2008, *A&A*, 486, 177  
 Zoccali, M., Vasquez, S., Gonzalez, O. A., et al. 2017, *A&A*, 599, A12

## Appendix A: Initial conditions & codes

The initial conditions of the two models explored in this study are obtained using the iterative method of Rodionov et al. (2009). The algorithm constructs equilibrium phase models for stellar systems, using a constrained evolution so that the equilibrium solution has a number of desired parameters, in our case the density distribution of the discs (see table A), which are modelled as Miyamoto-Nagai profiles, and the density distribution of the dark matter halo, which is modelled as a Plummer sphere (Binney & Tremaine 2008).

Simulation M2 was run with the Tree-SPH code of Semelin & Combes (2002), in which gravitational forces are calculated using a hierarchical tree method (Barnes & Hut 1986). A Plummer potential is used to soften gravity at scales smaller than  $\epsilon = 150$  pc. The equations of motion are integrated using a leapfrog algorithm with a fixed time step of  $\Delta t = 0.25$  Myr. The live dark matter halo has  $5 \times 10^5$  particles and a total mass of  $1.61 \times 10^{11}$  with a Plummer radius of 10 kpc, and the disc has  $1 \times 10^6$  particles. For a full description of the code the reader is referred to Semelin & Combes (2002).

Simulation M1 was run with a recently developed parallel MPI Tree-code which takes into account the adaptive spatial decomposition of particle space between nodes. The multi-node Tree-code is based on the 256-bit AVX instructions which significantly speed up the floating point vector operations and sorting algorithms (Khoperskov et al. in prep). The softening for model M1 is  $\epsilon = 50$  pc. In total the disc components of M1 have  $10 \times 10^6$  particles and the live dark matter halo is assigned  $5 \times 10^6$  particles with a total mass of  $3.68 \times 10^{11}$  with a Plummer radius of 21 kpc.

## Appendix B: Evolution in time

In Figure B.1 we show metallicity maps in  $l, b$  for the two models for three different snapshots, at the start of the simulation (top panels), after the bar forms (middle panels) and after the b/p bulge forms (bottom panels). We see that for model M1 the vertical gradient is present from the beginning of the simulations due to the vertically structured nature of the disc. This vertical negative gradient changes in steepness due to the formation of the b/p bulge, which increases the heights to which the metal-rich populations reach. In model M2 on the other hand there is no vertical gradient to begin with, and this is induced by the formation of the bar and b/p bulge.

This can be further understood by examining Figure B.2 where we show the fractional contribution (in surface density) of the three co-spatial discs of model M1 before (left panel Figure B.2) and after (right panel Figure B.2) the b/p bulge forms. We see that the vertical separation in populations is present from initial times, but that the coldest population ( $D1$ ) is puffed up after the formation of the b/p bulge, as the stars from this population are trapped more strongly in the bar-b/p instability and thus form a more prominent X-shape.

We see that the population  $D1$ , the thin disc population, is confined close to the plane where it dominates, whereas, as we move further away from the plane, the thick disc ( $D3$ ) contribution become more and more important especially above latitudes of  $|b| \sim 10$ . The contribution from the intermediate disc ( $D2$ ) is approximately constant at all the latitudes explored.

M1		$r_D$ (kpc)	$h_z$ (kpc)	$M$ ( $M_\odot$ )	$n_p$	[Fe/H] (dex)	$\sigma_{[Fe/H]}$ (dex)
	<i>Thin</i> (D1)	4.8	0.15	$4.21 \times 10^{10}$	5000000	0.3	0.15
	<i>Intermediate</i> (D2)	2	0.3	$2.57 \times 10^{10}$	3000000	-0.3	0.2
	<i>Thick</i> (D3)	2	0.6	$1.86 \times 10^{10}$	2000000	-0.65	0.2
M2							
	<i>Thin</i>	4.7	0.3	$10 \times 10^{10}$	1000000	$0.6 - 0.4 \times r$	-

**Table A.1.** Properties of the simulations used in this study. From left to right: the characteristic radius of the population, the characteristic height of the population, mass of the component, number of particles in component, the mean metallicity of the component and the dispersion in metallicity.

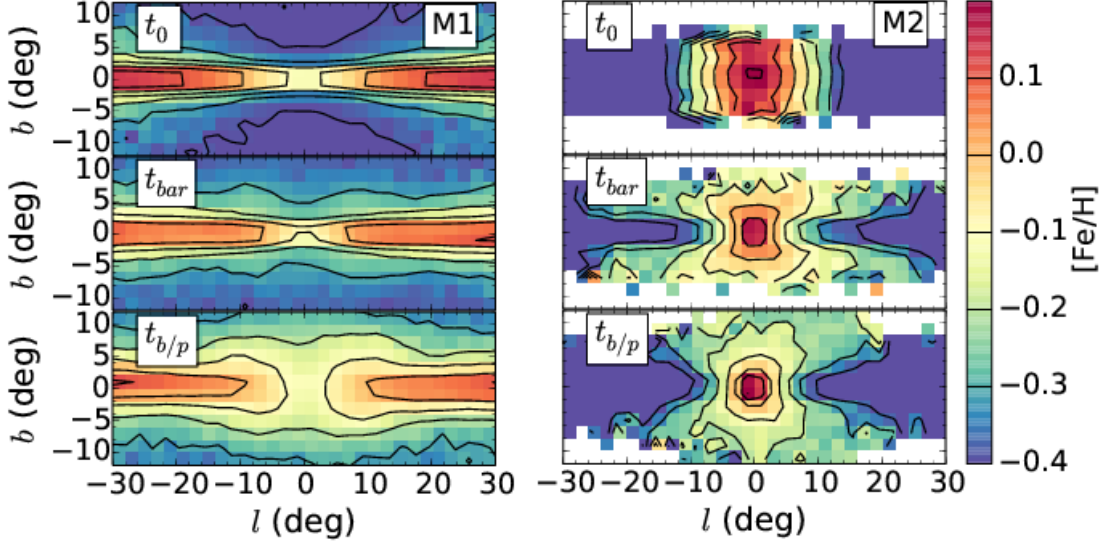


**Fig. B.1.** Metallicity maps in  $l, b$  for model M1 (left) and model M2 (right) at the start of the simulation  $t_0$  (top panels), after bar formation  $t_{bar}=3$  Gyr (middle panel) and after the bar buckles and the b/p forms  $t_{b/p}=5.5$  Gyr (bottom panel).

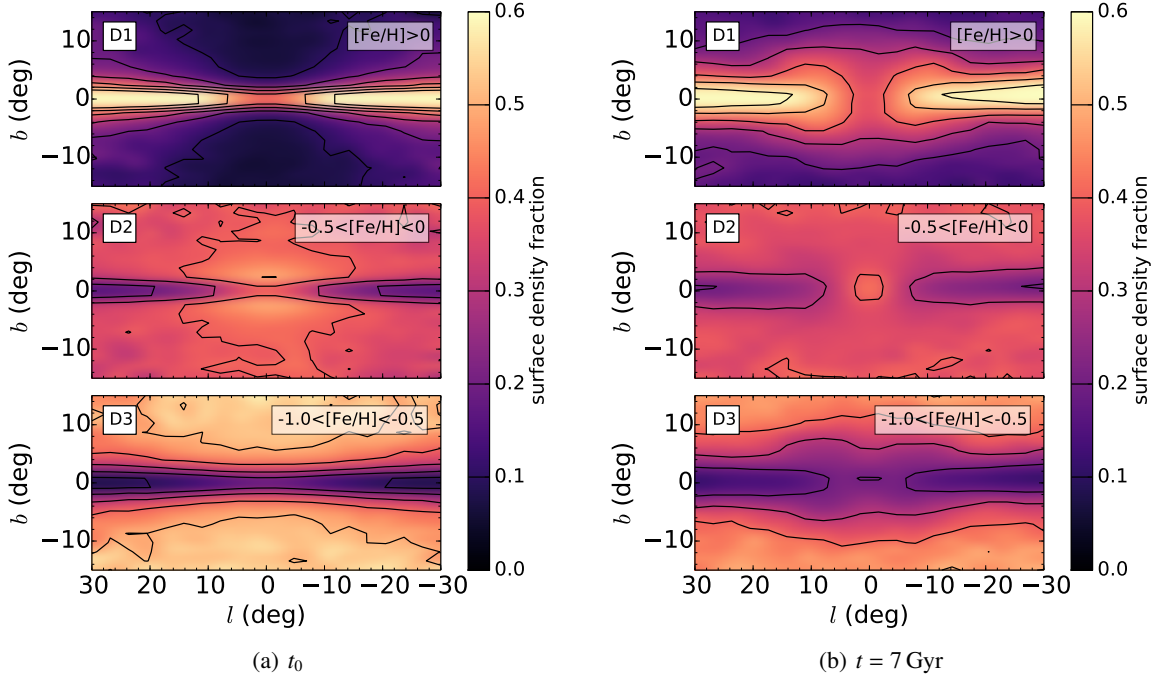


**Fig. B.2.** For model M1: Fractional contribution of each of the co-spatial discs along the line of sight in  $l, b$  for a snapshot at  $t=0$  (left) and at 7 Gyr (right, i.e. the same snapshot as the one shown in Figure 1) where we chose only particles with distances between 4 and 12 kpc from the Sun. At late times (right panel) the cold population, D1, puffs up and has a distinctive peanut shape.